Applied Energy 375 (2024) 124119

Contents lists available at ScienceDirect

Applied Energy

journal homepage: www.elsevier.com/locate/apenergy

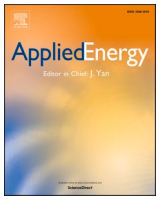

Probabilistic assessment method of small-signal stability in power systems based on quantitative PSS analysis

Hao Quan *, Wenyu Wang, Shaojia Zhang, Yun Zou

Department of Electrical Engineering, School of Automation, Nanjing University of Science and Technology, Nanjing, Jiangsu 210094, China

HIGHLIGHTS

- The effectiveness of PSS in small-signal stability are revealed quantitatively.
- CD-PSO algorithm for PSS parameter optimization is proposed.
- A joint simulation framework for multi-machine systems with RES is presented.
- A probabilistic assessment method of small-signal stability is proposed.
- Sensitivity analysis of RES penetration rates and load levels is implemented.

ARTICLE INFO

Keywords:
Small-signal stability
Probabilistic analysis
Power system stabilizer
Renewable energy penetration

ABSTRACT

Due to the exhaustion of fossil fuel energy and the awareness of environmental protection, the proportion of renewable energy sources (RES) integrated to the grid is increasing rapidly. However, the uncertainty of RES poses great challenges to the stability of power systems. To solve this uncertainty problem, power system small-signal stability analysis is transitioning from deterministic methods to probabilistic methods. Power system stabilizers (PSS) are important components to suppress low-frequency oscillations and improve system dynamic response performance. But there is still a lack of systematic simulation analysis regarding the optimization effect of PSS on probabilistic small-signal stability. In response to this problem, this paper proposes a probabilistic assessment method of small-signal stability based on quantitative PSS analysis. It constructs modified IEEE-14 and IEEE-39 bus systems with RES penetration and presents a joint simulation framework for multi-machine PSS parameter optimization based on the clustered difference mean perturbation particle swarm optimization (CD-PSO) algorithm. Then quantitative analysis is conducted on the impact of PSS integration on small-signal stability under a typical RES penetration rate (20%). Finally, the influence of different RES penetration rates and load levels on small-signal stability of power systems under different PSS scenarios is investigated.

1. Introduction

With the proposal of carbon peaking and carbon neutrality goals, the vigorous development of renewable energy is becoming an important means to cope with energy resource shortages, environmental degradation, and climate change [1,2]. While large and medium-sized hydropower plants have relatively good regulation capabilities, wind power and solar power generation have poor controllability. Their volatility and randomness bring a lot of uncertainty to the power system, posing great challenges to the safe and stable operation of the grid [3–5]. Small-signal stability in power systems has gradually gained attention. Power system simulation analysis is the foundation for power system planning, design, and dispatching operation [6]. In order to adapt to the development of smart grids, the power system needs to be modeled and simulated to make a guarantee for the stable operation of the power grid. Small-signal stability is an important component of power system stability assessment, which refers to the ability to maintain synchronization under small disturbances [7,8]. Since small disturbances in power systems are often difficult to detect, conducting rotor angle stability studies through modal analysis to ensure the damping of critical modes within recommended thresholds is crucial for ensuring the integrity of power systems with increasing shares of renewable energy sources (RES) [9].

In terms of small-signal stability analysis, reference [10] addressed the issue of small-signal stability mode analysis by proposing a method involving algebraic variables in power system mode determination and

* Corresponding author.
E-mail address: quanhao@njust.edu.cn (H. Quan).

https://doi.org/10.1016/j.apenergy.2024.124119
Received 14 May 2024; Received in revised form 8 July 2024; Accepted 31 July 2024
Available online 8 August 2024

Nomenclature

Variables

A	Coefficient matrix of the state equation system
ΔX	Column vector of state variable offsets
$p_1, p_2, \ldots, p_n$	Distinct roots of the characteristic equation
σ_n	The real part of a certain modal eigenvalue
ω_n	The imaginary part of a certain modal eigenvalue
f_n	The damping frequency
ζ_n	The damping ratio
p_w	The output power of the wind farm
v_{in}	The cut-in wind speed
v_{out}	The cut-out wind speed
v_r	The rated wind speed
p_{wr}	The rated power of the wind farm
G_{std}	The irradiance required for the photovoltaic module to reach its rated power under standard conditions
R_c	A specific irradiance point (120 W/m^2 in this study)
ζ_{th}	The minimum acceptable damping ratio threshold
ζ_{sys}	The minimum damping ratio under system oscillation mode
Tw	The washout time constant of the PSS
y_lim	The output limiting value of the PSS
K	The gain parameter of the PSS
$T1, T2, T3, T4$	The time constant of the PSS
w	The inertia weight
w_adapt	Weights changing with the number of iterations.
c_1, c_2	The acceleration constants
X_i	The position of the particle
V_i	The velocity of the particle
$pbest$	The personal best of individual particle.
$gbest$	The global best particle
$gbest\_avg$	The dimensional mean of the global best particle
$normal\_avg_i$	The dimensional mean of the i-th particle
$diff\_\overrightarrow{v_i}$	Scaled disturbance factor

Abbreviations

CD-PSO	Clustered difference mean perturbation particle swarm optimization
DFIG	Doubly fed induction generators
DPL	DIgSILENT Programming Language
DR	Damping ratio
MCS	Monte Carlo simulation
PDF	Probability density function
PSS	Power system stabilizer
PV	Photovoltaic
Real	Real part of eigenvalues
RES	Renewable energy sources
SSSC	Static synchronous series compensator

presenting a theorem for handling eigenvalue multiplicity without considering RES penetration. Based on the characteristics of photovoltaic systems, reference [11] derived a mathematical model suitable for distribution systems, conducted an eigenvalue analysis for different levels of photovoltaic penetration, and compared the results to evaluate the stability of the system. While various scenarios of RES penetration were considered in the previous study, the aforementioned studies are all based on deterministic system operating conditions, often with specific load scenarios and constant network configurations, without considering the uncertainty of RES. With the increase of distributed energy sources and dynamic loads, the evolution of interconnected power grids may cause underlying oscillations that affect certain key modes, which may lead to system collapse. Therefore, it is of great significance to conduct a probabilistic analysis of small-signal stability under various levels of RES penetration.

Currently, there are mainly two types of methods for probabilistic analysis of small-signal stability: the analytical methods and the simulation-based methods, such as the Monte Carlo simulation (MCS). Analytic methods are based on results obtained by processing analytic expressions of random variables without any form of sampling. However, their performance may degrade in the case of asymmetric distributions. Moreover, their outputs are various order moments, and their expansion may introduce accuracy issues [12,13]. Reference [14] studied the impact of wind power fluctuations on the probabilistic small-signal stability of the system using Gram-Charlier series and system eigenvalue sensitivity. Although analytical methods can avoid the computational burden associated with simulation-based methods, they typically require complex mathematical analysis. In terms of the MCS method, reference [15] proposed a hybrid method for probabilistic small-signal stability assessment of power systems based on clustering method and MCS, which improves the computational speed of MCS. Reference [16] proposed a probabilistic risk assessment framework for high-penetration renewable energy power systems, which is implemented through the MCS to generate a database of critical modes and quantify the stability risk associated with a high PV-integrated power grid using modal analysis and a risk matrix to capture the behavior of all critical modes. However, the aforementioned literature on probabilistic small-signal stability tends to study only a single scenario with or without PSS, lacking simulation analysis and comparison of the effectiveness of PSS. PSS is an auxiliary control device on synchronous generators, generally used in conjunction with the excitation system of the synchronous generator, which serves to provide control signals to enhance the system damping and to extend the power transfer limits so as to maintain the reliable operation of the power system [17]. Installing PSS in the excitation system of generators to provide positive damping is an effective measure to enhance the small-signal stability of power systems [18]. This paper focuses on revealing the effectiveness of PSS in general and conducting comparative analysis on the probabilistic small-signal stability of power systems with RES under different PSS scenarios.

The optimization performance of PSS is greatly influenced by its structure and parameters. Currently, much work has been done in this area. Some of these studies have focused on optimizing the structure and control methods of PSS [19,20]. Others have approached the optimization of PSS as a parameter tuning problem. In reference [21], Prony algorithm was utilized to identify the electromechanical mode of low-frequency oscillation of the system, and then the improved bat algorithm was employed to optimize the parameters of PSS. Reference [22] proposed a novel robust disturbance observer-based sliding mode controller for PSS and optimized the parameters using a multi-objective grasshopper optimization algorithm. In addition, beetle swarm algorithms [23], artificial fish swarm algorithms [24], fuzzy gravitational search algorithms [25], and other optimization algorithms have also been applied to parameter optimization for PSS. This paper focuses on the application of the particle swarm optimization (PSO) algorithm. In reference [26], an indirectly adaptive fuzzy coordinated PSS was designed and its parameters were optimized using a standard PSO algorithm. Reference [27] set the optimization objective as the system's ability to track a given value with minimal error in the system output and used PSO with changed weights for optimization. However, the aforementioned studies only considered the single-machine PSS scenario. In multi-machine systems, there are multiple electromechanical oscillation modes, and there exists coupling of damping between them. Designing the parameter of a PSS to limit a specific electromechanical oscillation mode may also affect the design of PSS for other oscillation

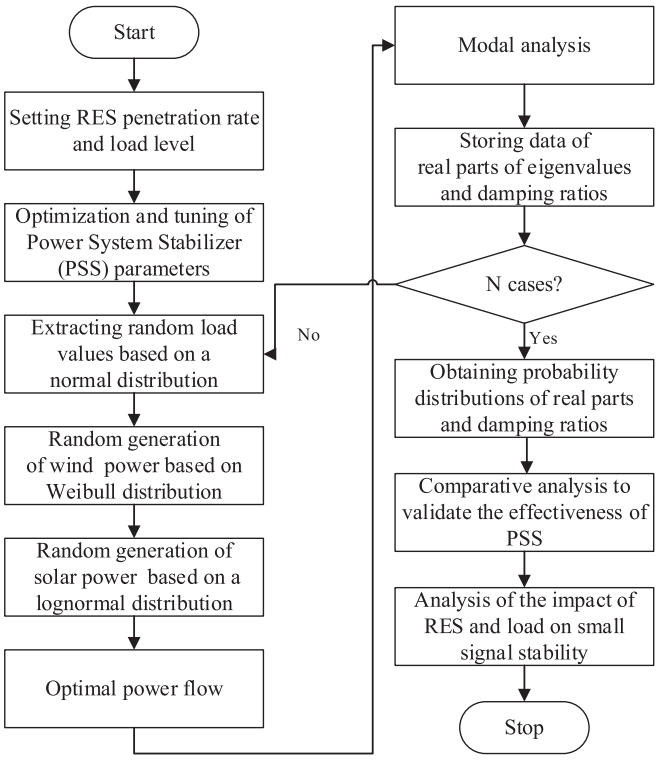

Fig. 1. Flowchart of probabilistic assessment method of small-signal stability considering RES uncertainty.

modes. Reference [28] considered the multi-machine scenario, transformed the PSS parameter tuning problem into a multi-objective function optimization problem based on eigenvalues and solved it using a standard PSO algorithm. A multi-objective PSO is also employed in reference [29]. In reference [30], PSS parameter optimization was conducted for systems including doubly fed induction generators (DFIG), and the update formula for particle velocity in the PSO algorithm was optimized to enhance the group's search capability. The optimization algorithm proposed in this paper, based on the standard PSO, further incorporates perturbation based on differential mean to enhance exploratory performance and diversity, making it more suitable for solving the multi-machine PSS system parameter tuning problems.

From the above literature reviews, we can see that: (1) It is necessary to conduct probabilistic small-signal stability analysis for different RES penetration rates. (2) The general effectiveness and necessity of PSS in small-signal stability simulation analysis of power systems need to be further explored. (3) Tuning method of multi-machine PSS parameters based on intelligent algorithms can be improved. This paper proposes a probabilistic assessment method of small-signal stability in power systems based on the Monte Carlo method considering the uncertainty of RES. The uncertainties of wind energy, solar energy, and load are modeled, and a joint simulation framework for PSS parameter optimization based on improved particle swarm optimization algorithm is presented. After verifying the effectiveness of PSS, the stability of the power system is quantitatively evaluated by analyzing the probability distribution changes of the real part and the damping ratio of the eigenvalues of the power system under different levels of RES penetration. The main contributions of this paper are as follows:

(1) The general effectiveness and necessity of PSS in small-signal stability simulation analysis of power systems are revealed.
(2) A PSS parameter optimization method based on the clustered difference mean perturbation particle swarm optimization (CD-PSO) algorithm is proposed.
(3) A joint simulation framework for PSS parameters in multi-machine systems based on the CD-PSO algorithm is proposed.
(4) The impact of different RES penetration rates and load levels on the probabilistic analysis of small-signal stability of PSS-based power systems is extended and investigated.

The rest of this paper is organized as follows. Section 2 presents the process of small-signal stability probabilistic assessment considering the integration of PSS and the uncertainty of RES. Section 3 describes the construction of the testing network and the modeling of RES uncertainty. Section 4 introduces the simulation framework for multi-machine PSS parameter joint optimization based on the proposed CD-PSO algorithm. The results and discussions are presented in Section 5, followed by a conclusion in Section 6.

2. Probabilistic assessment method for small-signal stability considering the uncertainty of RES

This section describes the proposed probabilistic assessment method for small-signal stability. The method utilizes the framework of MCS for probabilistic assessment of unstable risks related to power system oscillatory performance. The process of the proposed method is illustrated in Fig. 1. This method belongs to the simulation-based method, where the MCS process involves repeated sampling from the probability density function (PDF) of uncertain input variables to generate different scenarios, and then evaluates the system's oscillatory stability through modal analysis and storage of eigenvalue-related information. Modal analysis is generally performed using the QR/QZ method or the Arnoldi/Lanczos method. The Arnoldi/Lanczos method only computes a subset of eigenvalues, making it suitable for solving eigenvalues and eigenvectors of large sparse matrices [31]. In the proposed framework, the QR/QZ method is used for modal analysis. The proposed probabilistic assessment method of small-signal stability is implemented using the built-in programming language (DIgSILENT Programming Language, DPL) of DIgSILENT PowerFactory software.

2.1. Theoretical preparation

Small disturbances usually refer to normal load fluctuations, system operations, small load injections and removals, and system switching, etc. According to the Lyapunov stability theory, the stability of undisturbed motion can be determined by the properties of the roots of the characteristic equation of the linearized differential equation system describing the disturbed motion [32]. The linearized differential equation system can be represented as Eq.1:

$$\frac{d\Delta X}{dt} = A\Delta X, \tag{1}$$

where A is the coefficient matrix of the state equation system, and ΔX is the column vector of state variable offsets.

The characteristic equation is given by

$$det[A - pI] = 0, \tag{2}$$

The characteristic polynomial Eq.3 can be obtained by expanding Eq.2.

$$\alpha_0 p^n + \alpha_1 p^{n-1} + \cdots + \alpha_{n-1} p + \alpha_n = 0, \tag{3}$$

Let$p_1, p_2, \ldots, p_n$ be the n distinct roots of the characteristic equation, then there is a generalized solution of the following form:

$$x_i(t) = k_{i1} e^{p_1 t} + k_{i2} e^{p_2 t} + \cdots + k_{in} e^{p_n t}, \tag{4}$$

The characteristics of the solution to differential Eq. 1 depend entirely on the properties of the roots$p_1, p_2, \ldots, p_n$ of the characteristic equation.

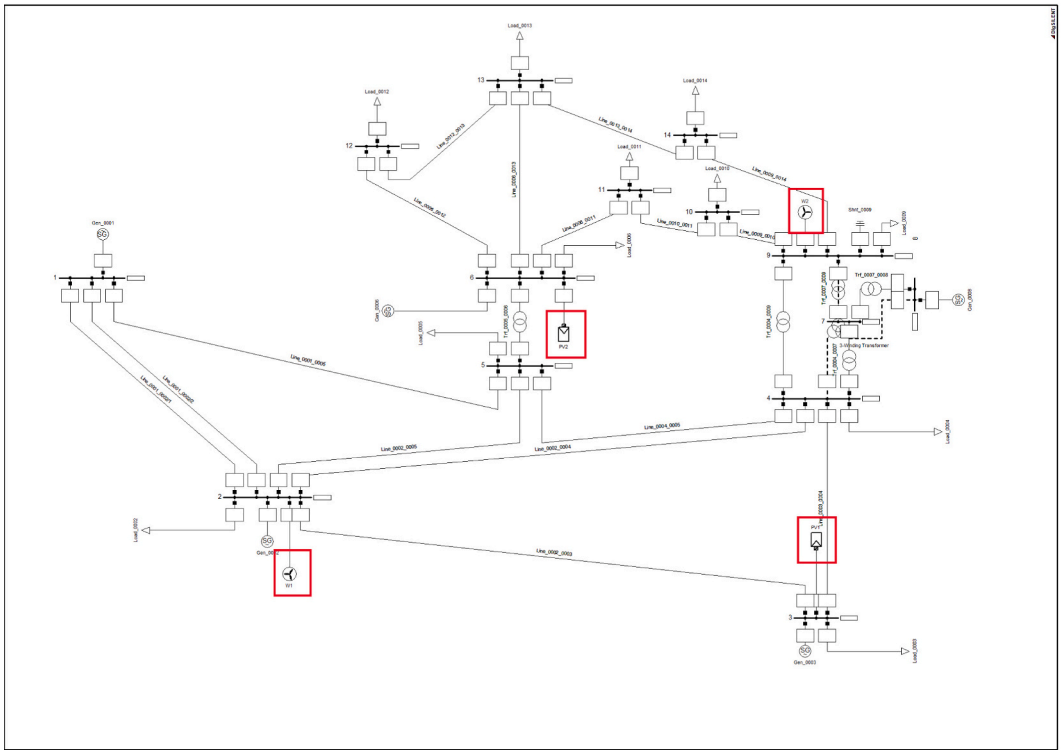

(a) Modified IEEE-14 system

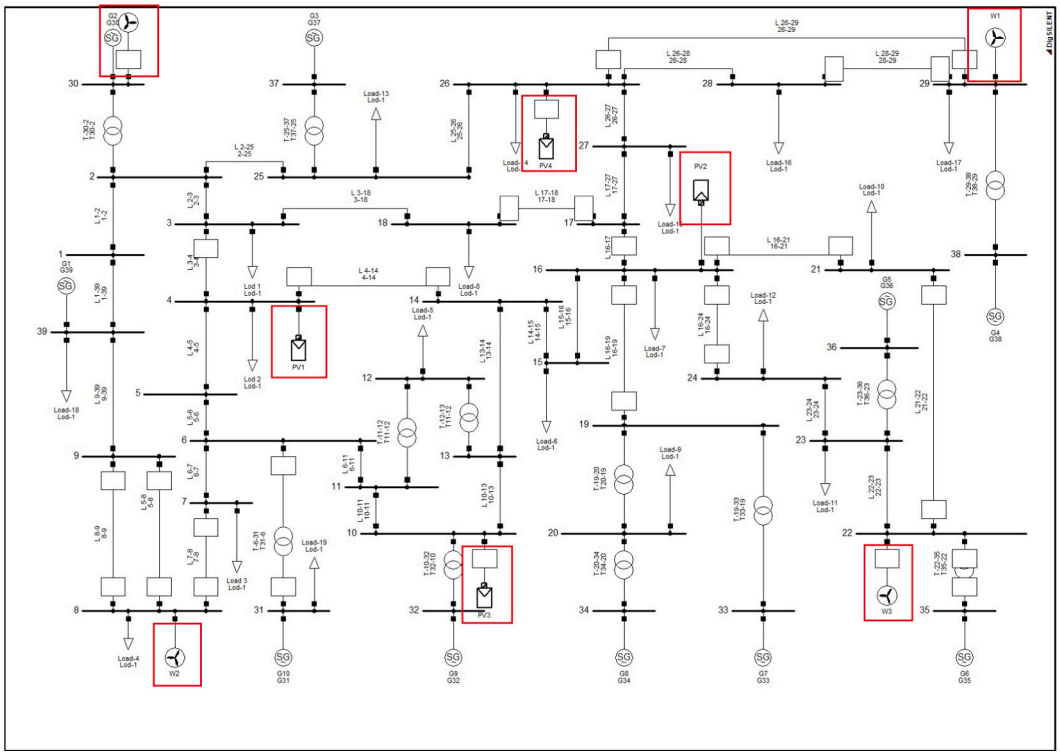

(b) Modified IEEE-39 system

Fig. 2. Modified IEEE-14 and IEEE-39 system with RES penetration.

$$p_n = \sigma_n + j\omega_n, \tag{5}$$

$$f_n = \frac{\omega_n}{2\pi}, \tag{6}$$

$$\zeta_n = -\frac{\sigma_n}{\sqrt{\sigma_n^2 + \omega_n^2}}, \tag{7}$$

where σ_n and ω_n represent the real and imaginary parts of a certain modal eigenvalue, f_n denotes the damping frequency, and ζ_n represents the damping ratio of the same mode.

When the real parts of the roots of the characteristic polynomial are negative, the system is stable. The damping ratio is a parameter that describes the magnitude of damping in an oscillatory system and reflects the rate of decay of oscillations after disturbances. When the damping ratio is negative, the system is unstable, and when the damping ratio is positive, a larger value indicates faster decay of oscillations and better small-signal stability of the system. The magnitude of the oscillation frequency reflects the response speed of the system after being disturbed. A higher frequency indicates a faster response speed. The higher the frequency, the faster the response speed.

2.2. Identification of critical modes

One of the main issues in small-signal stability analysis of power systems is to determine the extent of exposure to low-damping low-frequency oscillations, which typically occur in the range of 0.1 Hz to 1.0 Hz [33]. Small-signal instability in power systems usually occurs due to insufficient damping torque, which leads to an increase in rotor angle oscillation amplitude. Insufficient damping can have negative impacts on the power system. However, detecting such low frequency oscillations is challenging, and can only be identified through modal analysis by examining the eigenvalues of the system matrix [34]. In this study, parameters related to the modes with minimum global damping are selected from the modal analysis results, filtering out the values of modes within the frequency range of 0.03 Hz and 4 Hz.

2.3. RES uncertainty handling

In the analysis of RES, effective forecasting algorithms can be utilized to enhance the prediction accuracy [35–37]. Detailed modeling of wind turbines and photovoltaic (PV) systems can also be conducted, along with the application of new control strategies to mitigate the impact of uncertainties [38]. As the focus of this paper lies in the probability distribution of small signal stability, a stochastic mathematical model is adopted for construction.

Wind energy application scenarios can be categorized into static and dynamic scenarios. Static scenarios are generated based on one or more independent random variables and are suitable for cases involving long-term statistical patterns, such as power and load. While dynamic scenarios involve multiple and interconnected random variables and are suitable for large-scale wind power dispatch problems [39]. A large amount of research has shown that wind speed in wind farms generally follows certain probability distribution models, including the Gumbel, Weibull, and Rayleigh distributions. The Rayleigh distribution is a single-parameter model, while the other two are dual-parameter models.

Solar photovoltaic (PV) modeling can be approached from two perspectives. One approach focuses on the PV component system parameters and uses mathematical equations to model the dynamic behavior of the PV power source. The other approach considers power system stability and establishes power output characteristic models, including Weibull distribution models, Beta distribution models, and clustering analysis models. Based on the long-term statistical patterns of solar irradiance distribution, PV power exhibits a bimodal distribution. By decomposing it into two unimodal distributions, it can be modeled using a Beta distribution. Both the log-normal distribution and the Beta distribution can respond well to its volatility.

Table 1
Nominal voltages of the IEEE-14 and IEEE-39 bus systems.

IEEE-14 system	
Bus 1- Bus 5	132 kV
Bus 6, Bus 9- Bus 14	33 kV
Bus 7	1 kV
Bus 8	11 kV
IEEE-39 system	
Bus 12	138 kV
Bus 20	230 kV
Bus 30- Bus 38	16.5 kV

2.4. Uncertainty analysis

In this paper, MCS is performed to generate a sufficiently large critical mode database for drawing probability density functions (PDF). Each iteration of the MCS includes modal analysis to generate the required eigenvalue data. This iterative process continues until the desired number of simulations for the MCS is reached. Considering the impact of uncertainty in power systems, the data of critical modes can be plotted on PDFs. In this study, the PDF graphs of the real parts of eigenvalues and the corresponding damping ratios will be used to illustrate the situation of power systems under given conditions. By comparing the PDF plots before and after small perturbations, changes in power system behavior and response due to variations in RES penetration or load can be observed.

However, in some cases, certain small perturbations may not lead to explicit changes in the PDFs. Therefore, this study also utilizes the mean value of the real part of eigenvalues and the percentage change in damping ratios for various scenarios as relevant indicators of small signal stability, as shown in Eq.8:

$$\%Change = \frac{\mu_1 - \mu_0}{\mu_0} \times 100\%, \tag{8}$$

where μ_0 and μ_1 represent the average values before and after the disturbance respectively.

3. Testing network construction

In this study, a modified IEEE-14 bus system and IEEE-39 bus system were constructed on the DigSILENT PowerFactory simulation platform. The IEEE-14 bus system consists of 14 buses, 5 generators, 11 loads, 16 lines, 5 transformers and one shunt, as shown in Fig. 2(a). The nominal frequency of the IEEE-14 bus system is 60 Hz. The model has been completed by assuming the following typical values as nominal voltages in Table 1. The IEEE-39 bus system consists of 39 buses, 10 generators, 19 loads, 34 lines and 12 transformers, as depicted in Fig. 2(b). The nominal frequency of the IEEE-39 bus system is 60 Hz, and the mains voltage level is 345 kV. For nodes at a different voltage level, the following nominal voltages have been assumed. More detailed information can be obtained from references [40, 41].

3.1. Integration of renewable energy sources

For the test network above, the penetration rate of RES is calculated based on the total capacity of the system. Four different penetration levels, ranging from 10% to 40%, are simulated by adding additional renewable energy capacity based on the total generation capacity. In the IEEE-14 bus system, two photovoltaic plants are connected to buses 3 and 6, while two wind farms are connected to buses 2 and 9. In the IEEE-39 bus system, four photovoltaic plants are connected to buses 4, 10, 16,

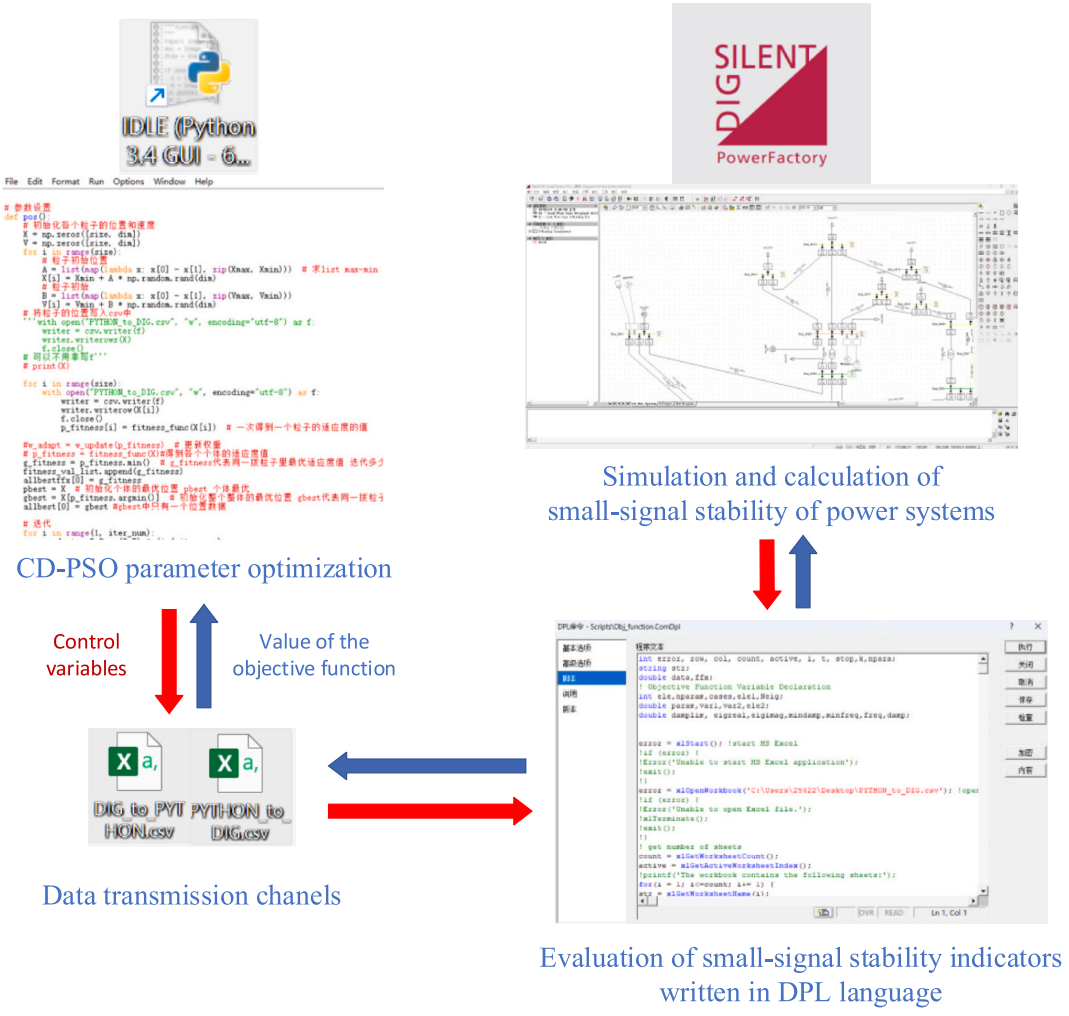

Fig. 3. Co-simulation framework for PSS parameter optimization.

and 26, and four wind farms are connected to buses 8, 22, 29, and 30, as shown in Fig. 2.

3.2. Uncertainty modeling

In this paper, it is assumed that the loads on different lines follow a normal distribution. The probability density function of the normal distribution is given by Eq.9:

$$f(x) = \frac{1}{\sqrt{2\pi}\sigma} e^{-\frac{(x-\mu)^2}{2\sigma^2}}, \tag{9}$$

where the mean $\mu = 1$ and the variance $\sigma^2 = 0.04^2$.

The wind speed distribution in the wind farm follows the Weibull distribution. The probability density function of the two-parameter Weibull distribution is shown in Eq.10:

$$f(x;\lambda,k) = \begin{cases} \frac{k}{\lambda}\left(\frac{x}{\lambda}\right)^{k-1} e^{-\left(\frac{x}{\lambda}\right)^k}, & x \geq 0 \\ 0, & x < 0 \end{cases}, \tag{10}$$

where λ is the scale parameter and k is the shape parameter. In this paper, the wind farms are set to $\lambda = 9$ and $k = 2$.

The output power of the wind farm p_w can be described as a function of wind speed v, as shown in Eq.11:

$$p_w(v) = \begin{cases} 0, v_{out} < v < v_{in} \\ p_{wr}\left(\frac{v - v_{in}}{v_r - v_{out}}\right), v_{in} \leq v \leq v_r \\ p_{wr}, v_r < v \leq v_{out} \end{cases}, \tag{11}$$

where the cut-in wind speed $v_{in} = 3$m/s, the cut-out wind speed $v_{out} = 25$m/s, the rated wind speed $v_r = 16$m/s, and the rated power of the wind farm $p_{wr} = 1$MW.

The solar irradiance distribution model adopts a lognormal distribution model. The apparent power of a single generator is 1 kVA, with a mean μ of 5.5 and a variance σ^2 of 0.6^2. The probability density function of the lognormal distribution is shown in Eq.12.

$$f(x,\mu,\sigma) = \begin{cases} \frac{1}{\sqrt{2\pi}\sigma x} e^{-\frac{1}{2\sigma^2}(\ln x - \mu)^2}, x > 0 \\ 0, x \leq 0 \end{cases}, \tag{12}$$

The conversion relationship between solar irradiance G (W/m^2) and output power is given by Eq.13.

$$P_s(G) = \begin{cases} P_{sr}\left(\frac{G^2}{G_{std}R_c}\right), 0 < G < R_c \\ P_{sr}\left(\frac{G}{G_{std}}\right), G \geq R_c \end{cases}, \tag{13}$$

In the equation above, $G_{std} = 800$W/m^2, which represents the

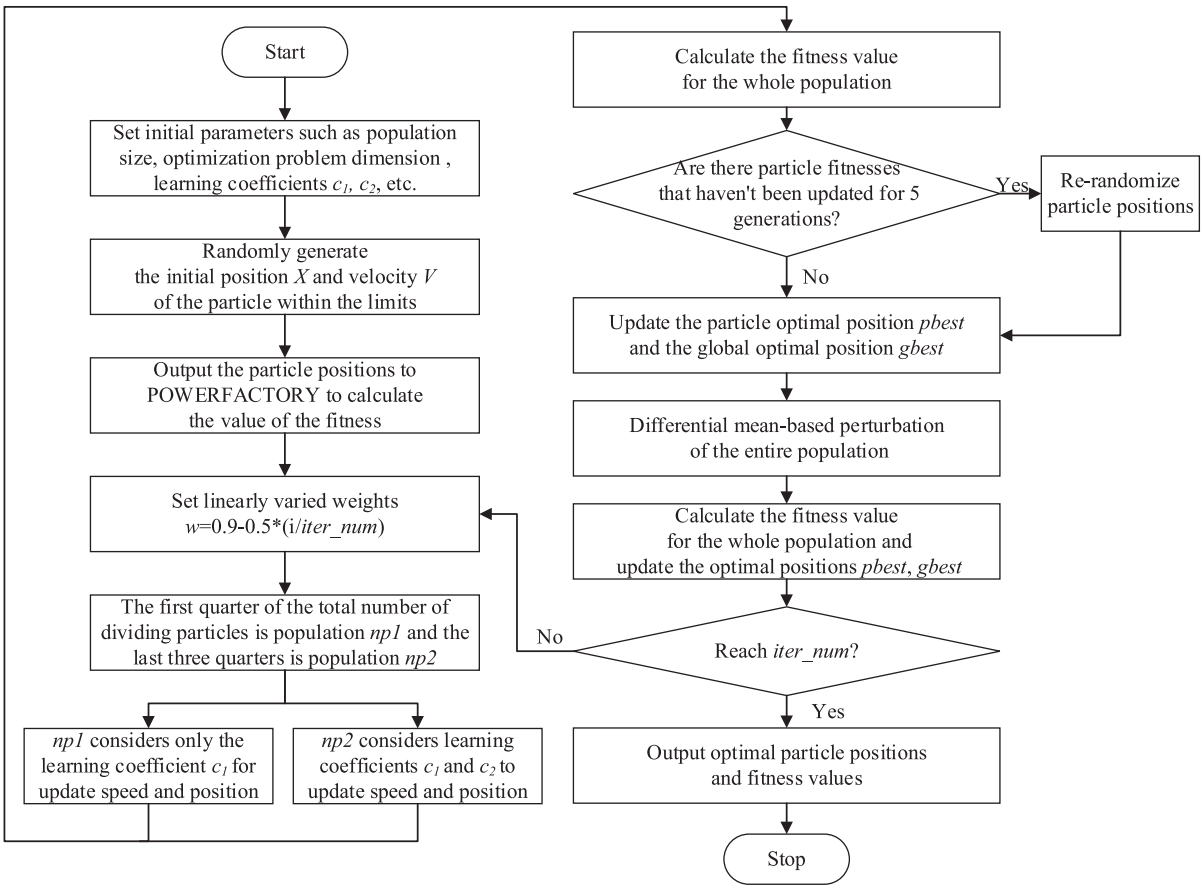

Fig. 4. Flowchart of CD-PSO algorithm.

irradiance required for the photovoltaic module to reach its rated power under standard conditions. R_c is a specific irradiance point, set to 120 W/m^2 in this study.

4. Power system stabilizer parameter tuning

The effectiveness of a PSS largely depends on the performance of its parameter settings. Therefore, it is necessary to configure the parameters of the PSS appropriately to achieve the desired system dynamic performance. In the aforementioned test networks, each generator is equipped with a PSS.

4.1. Joint simulation framework for PSS parameter optimization

Applying intelligent algorithms to the coordinated optimization of PSS parameters can greatly improve efficiency. This section proposes a joint simulation framework for PSS parameter optimization, as illustrated in Fig. 3. The intelligent algorithm is implemented, and the relevant parameters are set in Python. The evaluation of small-signal stability indicators is written in the built-in DIgSILENT Programming Language (DPL) of PowerFactory. The DPL language enables convenient control of the power system's parameter settings and simulation runs. During the simulation process, Python and DPL scripts can be called interchangeably, and data exchange between the two is facilitated through Excel as a data transfer channel.

In this paper, the objective function for the optimal parameter configuration of PSS in power systems is set as shown in Eq.14:

$$\begin{aligned} f &= min|\zeta_{th} - \zeta_{sys}| \\ \zeta_{sys} &= \min_{p=1\ldots nm}(\zeta_p) \end{aligned}, \tag{14}$$

where ζ_{th} represents the minimum acceptable damping ratio threshold, which is set to 15% in this paper, and ζ_{sys} represents the minimum damping ratio under system oscillation mode. The calculation of the objective function and the restrictions on the domain are implemented in the DPL script. The washout time constant Tw and the output limiting value y_lim are considered as known values, while the remaining parameters are optimized based on typical parameter restrictions, i.e., the gain parameter $K\in[0,100]$, the time constant $T1, T3\in[0.01, 0.2]$, and $T1/T2$, $T3/T4\in$ [1,15].

4.2. CD-PSO algorithm

Considering that the parameter setting of PSSs for multi-machine power systems is a multi-polar problem, this section proposes a Clustered Difference mean perturbation Particle Swarm Optimization (CD-PSO) algorithm. The flowchart of the CD-PSO algorithm is shown in Fig. 4. In general, the same velocity update formula Eq.16 is used for all particles within the particle swarm. This leads to direct information exchange between all particles and the global best member during each velocity and position update, which can result in a decrease in the diversity of the entire swarm and potentially lead to premature convergence. To address this issue, the population is divided into two parts, $np1$ and $np2$, and different velocity update formulas (Eq.15 and Eq.16) are used. This approach allows the $np1$ population to update its velocity without being influenced by the global best particle in order to enhance the exploratory capacity of the entire population.

Population $np1$:

$$V_{t+1} = w\_adapt^* V_t + {c_1}^* {r_1}^* (pbest - X_t), \tag{15}$$

Population $np2$:

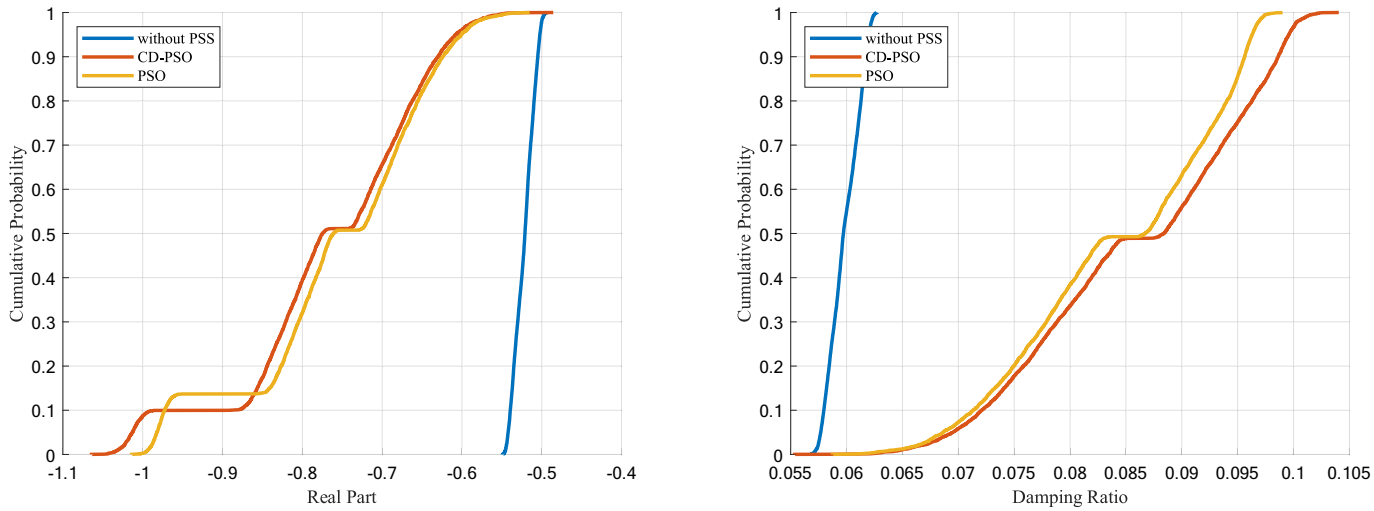

Fig. 5. Comparison of cumulative probabilities of real parts and damping ratio for different scenarios.

$$V_{t+1} = w\_adapt^{*} V_t + c_1{}^{*} r_1{}^{*} (pbest - X_t) + c_2{}^{*} r_2{}^{*} (gbest - X_t) \tag{16}$$

In addition, the scaled unit vector is superimposed on the current particle position to perturb the particle [42], and the steps are as follows:

1) Based on the current global best particle *gbest*, calculate the dimensional mean using Eq.17; calculate the dimensional mean of the *i*-th particle as in Eq.18.

$$gbest\_avg = \frac{1}{D} \sum_{j=1}^{D} \left(gbest_j \right) \tag{17}$$

$$normal\_avg_i = \frac{1}{D} \sum_{j=1}^{D} \left(X_{ij} \right) \tag{18}$$

where D represents the dimension of the search space, and j represents the j-th component.

2) Calculate the difference between the dimensional mean of the particle and the dimensional mean of *gbest*:

$$difference_i = gbest\_avg - normal\_avg_i \tag{19}$$

3) Randomly select a vector, normalize it, and scale it with $difference_i$.

$$diff\_\vec{v_i} = difference_i{}^{*} rand\_\vec{v} \Big/ \|\vec{v}\| \tag{20}$$

4) Add the scaled vector $diff\_\vec{v_i}$ to the i-th particle position X_i to obtain the perturbed particle position.

$$X_i^{'} = X_i + diff\_\vec{v_i} \tag{21}$$

On one hand, random unit vectors bring disturbances to the system, which can increase the diversity of the population. On the other hand, the closer a particle is to the global best particle, the smaller the disturbance it receives. This also preserves the attractiveness of the global best particle and prevents convergence problems.

5. Case study

This section analyzes the impact of PSS, the penetration rate of RES, and load increases on the stability of the modified IEEE-14 bus system and IEEE-39 bus system.

For the IEEE-14 bus system and IEEE-39 bus system, 30 case studies were conducted: 5 cases without PSS under base load conditions, 5 cases with PSS under base load conditions, 5 cases with a 5% load increase without PSS, 5 cases with a 5% load increase with PSS, 5 cases with a 10% load increase without PSS, and 5 cases with a 10% load increase with PSS. The five cases in each group are consisted of scenarios with base cases, which refer to scenarios where the penetration rate of RES is 0, and penetration levels range from 10% to 40%. In this section, small-signal stability analysis based on stochastic RES changes was performed with 5000 Monte Carlo simulations for each scenario.

5.1. Impact of PSS on small-signal stability

Fig. 5 illustrates the cumulative probability curves of the real parts and damping ratios for a system with a 20% penetration rate of RES in an IEEE-14 bus system. The three curves represent the cases without PSS, with PSS parameters obtained using the CD-PSO algorithm, and with PSS parameters obtained using the standard PSO algorithm. The PSS parameters were set to the values that yield the minimum damping ratio closest to the minimum acceptable damping ratio threshold for all oscillation modes under a 20% RES penetration scenario. A 20% RES penetration rate is applied in the parameter setting of PSSs because in our small signal stability analysis, the penetration rate of RES ranges from 0% to 40%, and 20% is a compromise value. In addition, in 2022, the proportions of wind and solar power generation in the United States and the European Union were 14.9% and 22.3%, respectively. As a result, 20% is considered to be a typical penetration rate.

The parameter setting of the CD-PSO algorithm includes a minimum value of 0.4 and a maximum value of 0.9 for the inertia weight w, with both c_1 and c_2 set to 2. For the IEEE-14 bus system, the search space dimension is set to 25, while for the IEEE-39 bus system, the search space dimension is set to 50. The number of particles is 40, and the number of iterations is 100.The standard PSO algorithm is configured with $w = 1$, $c_1 = 2$, $c_2 = 2$, a particle size of 40, and 100 iterations. The obtained PSS parameters are input into the power system, and five thousand Monte Carlo simulations are conducted under the condition of 20% RES installation capacity. The curves of Fig. 5 were plotted based on the results.

According to the Lyapunov stability theory, the closer the real part of the eigenvalues are to the left side of the x-axis and the closer the damping ratio curves are to the right side of the x-axis, the better the small-signal stability of the system. It can be observed that compared to the blue curve without PSS, the addition of PSS can improve the stability of the system effectively under a 20% RES penetration scenario. Furthermore, the optimization performance of PSS is influenced by its

Table 2
The percentage change of the indicators after the addition of PSS in IEEE-14 system.

	(a) Average real parts					(b) Average damping ratio				
	Base	10%	20%	30%	40%	Base	10%	20%	30%	40%
Base Load	73.18%	61.57%	46.68%	31.71%	16.70%	58.51%	52.58%	43.50%	30.93%	16.40%
Load +5%	76.90%	65.54%	51.04%	35.11%	19.77%	60.52%	54.71%	46.32%	33.71%	19.32%
Load +10%	80.57%	72.93%	59.11%	49.57%	22.84%	62.75%	59.14%	51.95%	45.46%	22.15%

Table 3
The percentage change of the indicators after the addition of PSS in IEEE-39 system.

	(a) Average real parts					(b) Average damping ratio				
	Base	10%	20%	30%	40%	Base	10%	20%	30%	40%
Base Load	67.89%	68.46%	56.23%	33.67%	11.43%	47.08%	47.71%	40.25%	24.14%	5.35%
Load +5%	68.70%	67.67%	65.12%	51.63%	30.99%	47.20%	46.68%	45.56%	38.14%	20.90%
Load +10%	68.19%	72.20%	67.06%	65.51%	35.78%	46.70%	49.54%	45.87%	46.78%	25.76%

Table 4
PSS parameters of IEEE-14 system obtained by CD-PSO tuning.

	Generator1	Generator2	Generator3	Generator4	Generator5
Kw	99.82027	98.6003	99.68134	99.31537	7.30909
T1	0.199695	0.116418	0.133432	0.160447	0.092672
T2	0.013462	0.008016	0.008924	0.015505	0.010713
T3	0.199957	0.110057	0.138729	0.10324	0.102854
T4	0.013434	0.007475	0.079249	0.007195	0.007568

parameters, and the parameters obtained using the CD-PSO algorithm are superior to those obtained using the standard PSO algorithm in the small-signal stability probability analysis.

Table 2 and Table 3 show the percentage change of various indicators after the addition of PSS under different conditions. In this case, let the value with PSS be X_{PSS}, and the value without PSS be X_0. The percentage calculation expression can be written as $(X_{PSS} - X_0)/X_0$. In the case of real parts, if the small signal power system is stable, the real parts of the eigenvalues should be negative. When the case with PSS is better, $X_{PSS} - X_0$ is a negative value. Since X_0 is also a negative value, the percentage change obtained by dividing is a positive value. The damping ratio can be calculated using the same formula. It can be seen that all values in the table are positive, which means the inclusion of PSS can effectively optimize the stability of the power system regardless of changes in RES penetration and load levels. Particularly, the optimization effect of PSS is significant at low RES penetration rates. However, as the penetration rate increases, the optimization effect gradually deteriorates, which may be due to the fact that the tuning performance of the PSS is set based on a single operating point, and the PSS parameters computed in the case of RES penetration of 20% do not guarantee the best optimization effect in all penetration rate cases. Therefore, it is necessary to adjust the PSS parameters promptly when there are significant changes in the penetration rate of RES to achieve the best optimization performance.

5.2. Impact of different RES penetration rates on small-signal stability

The nonlinear characteristics of power systems pose certain challenges to system analysis. The sensitivity analysis method can show the extent of changes in selected dependent variables caused by certain independent variables. This subsection's sensitivity matrix reflects the degree of change in each indicator from the base case to the case with a 40% penetration rate. The horizontal percentages represent the pre-change conditions, while the vertical percentages represent the post-change conditions.

As mentioned in Section 5.1, all indicators are better with PSS compared to without PSS. Therefore, this section only presents the PDF graphs of the real parts of eigenvalues and damping ratios for the IEEE-14 and IEEE-39 bus systems with PSS under the base load condition, as well as the sensitivity matrix. The parameters of PSS in the IEEE-14 bus system are shown in Table 4. The parameters of PSS in the IEEE-39 bus system are omitted here due to the space limitation.

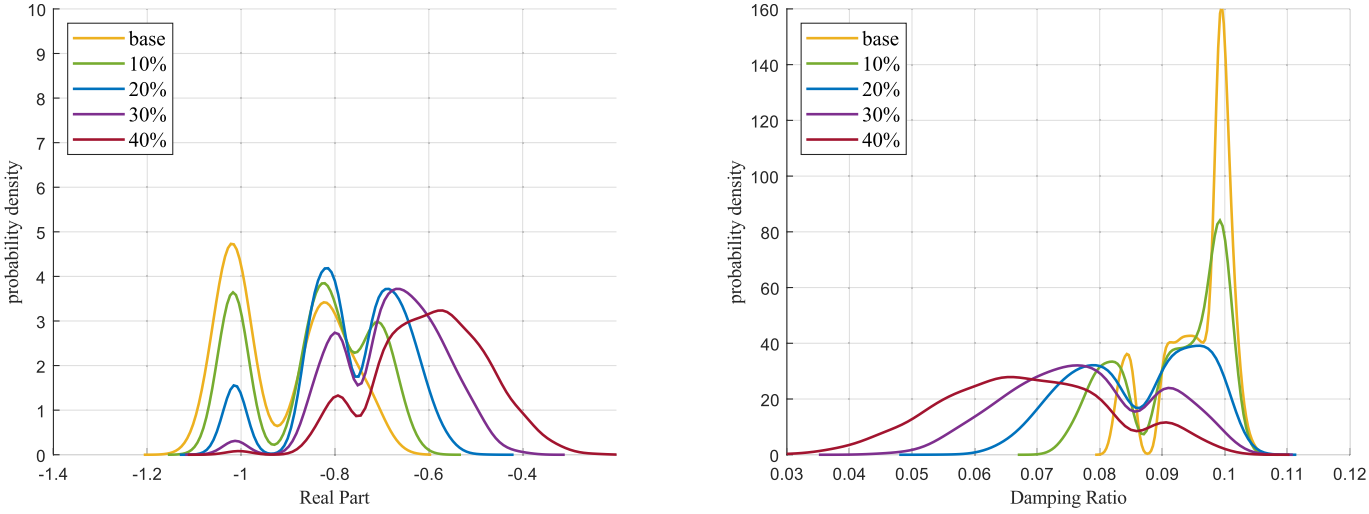

Fig. 6. PDF of different RES penetration rates in IEEE-14 system with PSS.

Table 5
Sensitivity matrix of IEEE-14 system with PSS under different RES penetration rates.

(a) Real parts

	Base	10%	20%	30%	40%
Base	0.00%				
10%	-6.92%	0.00%			
20%	-15.91%	-9.66%	0.00%		
30%	-25.20%	-19.65%	-11.05%	0.00%	
40%	-34.39%	-29.52%	-21.98%	-12.29%	0.00%

(b) Damping Ratio

	Base	10%	20%	30%	40%
Base	0.00%				
10%	-4.17%	0.00%			
20%	-10.43%	-6.53%	0.00%		
30%	-19.11%	-15.59%	-9.69%	0.00%	
40%	-28.82%	-25.72%	-20.53%	-12.01%	0.00%

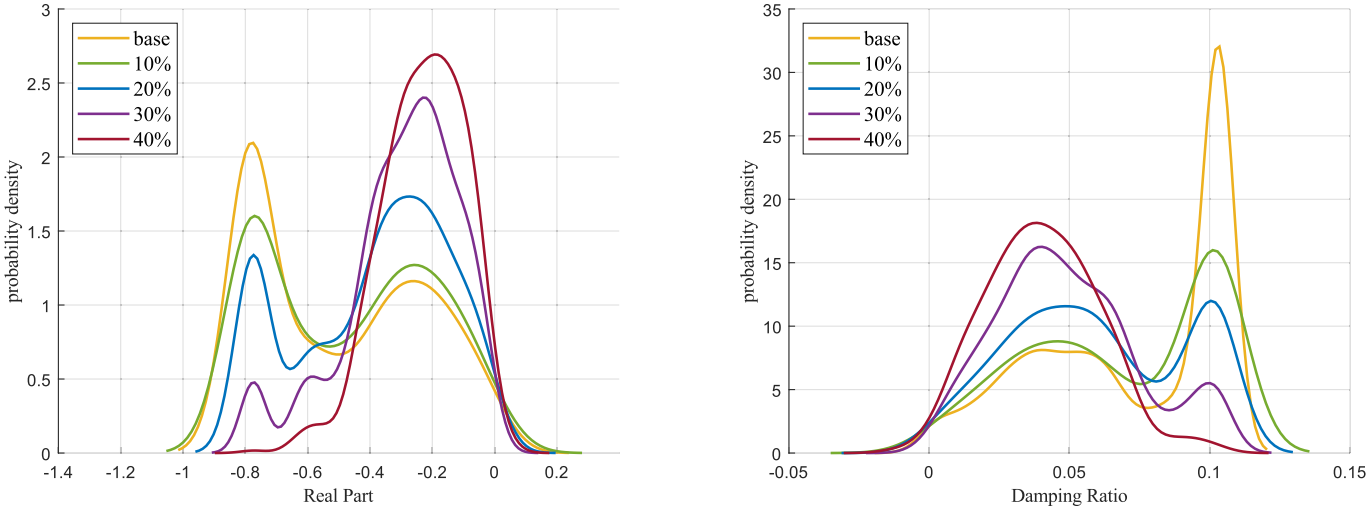

Fig. 7. PDF of different RES penetration rates in IEEE-39 system with PSS.

Fig. 6 shows the PDFs of the real part of the eigenvalues and the damping ratio of different RES penetration rates in the IEEE-14 bus system with PSS. Comparing Fig. 6, it can be seen that as the RES penetration increases, the curves in the real part show an overall rightward shifting trend, while the curves in the damping ratio show an overall leftward shifting trend, which represents a gradual decrease in the stability of the system. As the penetration rate of RES increases from 0 to 10%, the worst-case real part of the eigenvalues gradually shifts from the left of −0.6 to the right. This change becomes more prominent when the RES penetration rate of the test grid reaches 40%, with the real part of the most unstable condition being approximately −0.3. Such changes can be more intuitively observed in the curve of the damping ratio. This can also be observed through the sensitivity matrix as shown in Table 5, in which a negative number means that the situation is getting worse, and the negative values for all the above cases mean that the stability of the system decreases as the penetration rate of RES increases. The impact on system stability at 40% penetration levels shows a 34.39% and 28.82% shift in the mean values of the real parts and damping ratios, respectively, the greatest deviation between the cases. Due to the volatility and uncertainty of RESs, as the penetration rate of renewable energy increases, the system's unreliable volatility may lead to frequency instability and voltage fluctuations, thereby affecting the system's stability.

In addition, by examining the sensitivity matrix, it can be observed that the percentage change in the average value of the power system is directly proportional to the penetration rate of RES. The penetration rate of RES increased from 0% to 10%, resulting in a deterioration of the average real part of eigenvalues by 6.92%. With an increase from 30% to

Table 6
Sensitivity matrix of IEEE-39 system with PSS under different RES penetration rates.

(a) Real parts

	Base	10%	20%	30%	40%
Base	0.00%				
10%	-6.30%	0.00%			
20%	-21.88%	-16.63%	0.00%		
30%	-40.78%	-36.80%	-24.19%	0.00%	
40%	-54.19%	-51.11%	-41.36%	-22.65%	0.00%

(b) Damping Ratio

	Base	10%	20%	30%	40%
Base	0.00%				
10%	-5.03%	0.00%			
20%	-17.16%	-12.77%	0.00%		
30%	-32.43%	-28.85%	-18.44%	0.00%	
40%	-44.33%	-41.38%	-32.80%	-17.60%	0.00%

Table 7
Impact of load increases for different RES penetration rates in IEEE-14 systems.

Without PSS	Base	10%	20%	30%	40%	With PSS	Base	10%	20%	30%	40%
load+5%						load+5%					
Real	-0.07%	0.04%	0.11%	0.25%	0.24%	Real	2.07%	2.50%	3.08%	2.84%	2.88%
DR	-0.05%	0.10%	0.15%	0.27%	0.25%	DR	1.22%	1.50%	2.11%	2.40%	2.76%
load+10%						load+10%					
Real	-0.26%	-0.04%	0.19%	0.45%	0.45%	Real	4.00%	6.99%	8.68%	14.07%	5.74%
DR	-0.13%	0.08%	0.28%	0.49%	0.46%	DR	2.53%	4.39%	6.18%	11.64%	5.43%

Table 8
Impact of load increases for different RES penetration rates in IEEE-39 systems.

Without PSS	Base	10%	20%	30%	40%	With PSS	Base	10%	20%	30%	40%
load+5%						load+5%					
Real	0.17%	4.47%	8.14%	7.91%	4.91%	Real	0.65%	3.98%	14.30%	22.41%	23.33%
DR	0.38%	3.65%	6.14%	4.64%	1.74%	DR	0.47%	2.92%	10.15%	16.44%	16.76%
load+10%						load+10%					
Real	0.47%	5.63%	12.80%	15.61%	11.59%	Real	0.65%	7.97%	20.62%	43.15%	35.98%
DR	0.65%	4.65%	10.13%	10.40%	5.17%	DR	0.39%	5.95%	14.55%	30.54%	25.55%

40%, the deterioration reached 12.29%, which is nearly twice as much as the former case. The same situation can also be identified by observing the average value of the damping ratio. This means that when the penetration rate is high, increasing the penetration rate by the same percentage will pose greater challenges to the stability of the power system. With the increase in the penetration rate of RES, the dynamic characteristics of the system will undergo significant changes. In cases of lower penetration rates, the system can adapt well to the volatility of RES. However, with higher penetration rates of renewable energy, the impacts brought about will gradually exceed the stability boundaries of the system. The above conclusions can be verified in the IEEE-39 bus system in Fig. 7 and Table 6.

5.3. Impact of different load levels on small-signal stability

The rates of change of relevant indicators at different load levels are displayed in Table 7 and Table 8. Real represents the real part of eigenvalues, and DR represents the damping ratio. In Tables 7 and 8, the percentage calculation compares the indicator values obtained by increasing the load level with the values obtained at the base load level under the same RES penetration rate. Positive values indicate that the parameter values are better after the load increases compared to the base load condition. Overall, it can be seen that the small-signal stability improves as the load increases. It is worth noting that when the penetration rate of RES reaches 30%, the average values of the real part of eigenvalues and damping ratio undergo significant changes after load increase.

However, under low penetration rates of RES, an increase in power system instability may occur when the load increases. One possible reason for this is that when the load increases, the generators and transmission lines in the power system will bear a greater load, potentially approaching or exceeding their rated capacity. This can result in a slower dynamic response of the equipment, making it unable to adjust timely to adapt to load changes, thereby reducing the system's response capability and stability. If the increase in load leads to insufficient generation capacity in the power system, it may also result in power imbalance, causing voltage and frequency fluctuations, which have a negative impact on stability. With the integration of RES, this shortfall in generation capacity is compensated, leading to an improvement in system stability.

6. Conclusions

In this paper, a probabilistic analysis method for small-signal stability in power systems based on quantitative PSS analysis is proposed for power systems with different penetration levels of RES. For systems with PSS under typical RES penetration ratios, a joint simulation framework and CD-PSO algorithm are proposed for PSS parameter tuning in power systems. After verifying the effectiveness of PSS, the impact of different levels of RES integration on small-signal stability in the system is investigated. The strategies proposed in this paper are applied to the IEEE-14 and IEEE-39 bus systems, respectively. In the testing systems, the probabilistic distributions of the real part of eigenvalues and damping ratio are used as indicators to quantitatively evaluate the impact of changes in RES penetration rate and load level.

Based on the results of two testing systems, the following conclusions can be drawn:

1) The addition of PSS significantly improves the stability of the power system, especially at lower levels of RES penetration.
2) Regardless of PSS inclusion, higher levels of RES penetration generally lead to poorer system stability.
3) With sufficient RES supply, an increase in load generally benefits the stability of the power system, regardless of PSS inclusion.
4) The optimization effect of PSS decreases as the penetration rate of RES increases, which may pose instability risks to the grid. Therefore, it is necessary to recalibrate the parameters of PSS when there is a significant change in RES penetration rate.

It is worth noting that the modeling of wind and solar energy in the

article adopts stochastic mathematical models, ignoring the spatiotemporal correlation of wind and solar power generation scenarios, which may affect the validation of the experimental results. In addition, energy storage systems, as an important component of modern power systems, will be taken into account with RES together for their impacts on the grid stability in the future work.

CRediT authorship contribution statement

Hao Quan: Writing – review & editing, Resources, Project administration, Methodology, Funding acquisition, Conceptualization. **Wenyu Wang:** Writing – original draft, Visualization, Validation, Software, Investigation, Formal analysis, Data curation. **Shaojia Zhang:** Visualization, Investigation, Data curation. **Yun Zou:** Validation, Supervision, Software, Investigation.

Declaration of competing interest

The authors declare that they have no known competing financial interests or personal relationships that could have appeared to influence the work reported in this study.

Data availability

Data will be made available on request.

Acknowledgments

This work was supported in part by the Natural Science Foundation of Jiangsu Province, China under Grant BK20211195, and in part by the National Natural Science Foundation of China under Grant 51907090.

References

[1] Wu WC, Xu SW, Yang Y, Wang B, Lin CH, Shen YK. Risk-quantified probabilistic dispatch for power system with high proportion of renewable energy. Automf Elect Power Syst 2023;47(15):3–11.
[2] Ma Y, Li YP, Huang GH. Planning China's non-deterministic energy system (2021–2060) to achieve carbon neutrality. Appl Energy 2023;334:120673.
[3] Bai JH, Xin SX, Liu J, Zhen K. Roadmap of realizing the high penetration renewable energy in China. Proc CSEE 2015;35(14):3699–704.
[4] Gandhi O, Kumar DS, Rodriguez-Gallegos CD, Srinivasan D. Review of power system impacts at high PV penetration part I: factors limiting PV penetration. Sol Energy 2020;210:181–201.
[5] Chen F, Zhang WY, Chen R, Jiang FF, Ma J, Zhu XH. Adapting carbon neutrality: tailoring advanced emission strategies for developing countries. Appl Energy 2024; 361:122845.
[6] Tian F, Huang YH, Shi DY, Xia T, Qiu WJ, Hu XB, et al. Developing trend of power system simulation and analysis technology. Proc CSEE 2014;34(13):2151–63.
[7] Pareek P, Nguyen HD. Probabilistic robust small-signal stability framework using Gaussian process learning. Electr Power Syst Res 2020;188:106545.
[8] Kweon J, Jing H, Li Y, Monga V. Small-signal stability enhancement of islanded microgrids via domain-enriched optimization. Appl Energy 2024;353:122172.
[9] Nair DV, Murty MSR. Modal analysis of power system and study of oscillatory instability. In: 2016 2nd international conference on applied and theoretical computing and communication technology; 2016. p. 667–72.
[10] Tzounas G, Dassios I, Milano F. Modal participation factors of algebraic variables. IEEE Trans Power Syst 2020;35(1):742–50.
[11] Eftekharnejad S, Vittal V, Heydt GT, Keel B, Loehr J. Small signal stability assessment of power systems with increased penetration of photovoltaic generation: a case study. IEEE Trans Sustainable Energy 2013;4(4):960–7.
[12] Xu J, Kanyingi PK, Wang KY, Li GJ, Han B, Jiang XC. Probabilistic small signal stability analysis with large scale integration of wind power considering dependence. Renew Sust Energ Rev 2017;69:1258–70.
[13] Preece R, Huang K, Milanovic JV. Probabilistic small-disturbance stability assessment of uncertain power systems using efficient estimation methods. IEEE Trans Power Syst 2014;29(5):2509–17.
[14] Bu SQ, Du W, Wang HF. Probabilistic analysis of small-signal rotor angle/voltage stability of large-scale AC/DC power systems as affected by grid-connected offshore wind generation. IEEE Trans Power Syst 2013;28(4):3712–9.
[15] Madadi S, Mohammadi-Ivatloo B, Tohidi S. Probabilistic small signal stability evaluation of power systems with high penetration of wind farms. Comput Electr Eng 2020;85:106683.
[16] Kumar DS, Quan H, Wen KY, Srinivasan D. Probabilistic risk and severity analysis of power systems with high penetration of photovoltaics. Sol Energy 2021;230: 1156–64.
[17] Lu DQ, Yang XH, Guo RQ, Zhang GY, Liu YX. Parameter optimization of PSS based on genetic algorithm. Chinese J Power Sources 2013;37(10):1843–5.
[18] Feng N, Guo LJ, Fu JW, Ma J. Research summary of power system stabilizer. Shaanxi Elect Power 2013;41(11):45–50.
[19] Mujeer SA, Dwarasila MK, Chintala JD, Adimulam VSK. Low frequency oscillations damping by design of power system stabilizer using intelligent controllers. Mater Today: Proc 2023;80(3):2862–71.
[20] Ray PK, Paital SR, Mohanty A, Eddy FYS, Gooi HB. A robust power system stabilizer for enhancement of stability in power system using adaptive fuzzy sliding mode control. Appl Soft Comput 2018;73:471–81.
[21] Zhao F, Guo CL, Si JJ. Research on optimization of PSS parameters based on bat algorithm. Control Engf China 2018;15(12):2210–8.
[22] Falehi AD. Optimal robust disturbance observer based sliding mode controller using multi-objective grasshopper optimization algorithm to enhance power system stability. J Ambient Intell Humaniz Comput 2020;11:5045–63.
[23] Wang YH, Zhang W. Optimization of multi-machine PSS parameters based on beetle swarm optimization algorithm. Control Engf China 2022;29(8):1345–51.
[24] Hu XB, Yang LM, Chen Z, Wang HF, Tang GQ. PSS parameter optimization based on artificial fish-swarm algorithm29(2); 2009. p. 47–50.
[25] Ghasemi A, Shayeghi H, Alkhatib H. Robust design of multimachine power system stabilizers using fuzzy gravitational search algorithm. Electr Power Energy Syst 2013;51:190–200.
[26] Bouchama Z, Harmas MN. Optimal robust adaptive fuzzy synergetic power system stabilizer design. Electr Power Syst Res 2012;83(1):170–5.
[27] Wu F, Chen WR, Li Q, Lu XF. Parameter optimization of power system stabilizer on particle swarm optimization algorithm. Power Syst Prot Control 2009;37(10):53–8.
[28] Shayeghi H, Shayanfar HA, Safari A, Aghmasheh R. A robust PSSs design using PSO in a multi-machine environment. Energy Convers Manag 2010;51(4):696–702.
[29] Falehi AD, Mosallanejad A. Neoteric HANFISC-SSSC based on MOPSO technique aimed at oscillation suppression of interconnected multi-source power systems. IET Gener Transm Distrib 2016;10(7):1728–40.
[30] Derafshian M, Amjady N. Optimal design of power system stabilizer for power systems including doubly fed induction generator wind turbines. Energy 2015;84: 1–14.
[31] Amaral Jr TS, CLT SG Borges. Reliability evaluation of bulk power systems with wind generation using small signal stability analysis. Int J Electr Power Energy Syst 2021;129:106840.
[32] Zhao JJ, Zuo LL, Zhao LG, Huang SY. Study on voltage control strategy of DFIG in microgrid and small-disturbance voltage stability analysis. Elect Mach Control Appl 2018;45(3):22–9.
[33] Gonzalez-Longatt FM, Rueda JL. Powerfactory applications for power system analysis. Switzerland: Springer; 2014.
[34] Wang HX, Liu MQ, Dong HN, Lu SY, Yang ZH, Chen SS, et al. Review on analysis and suppression of low-frequency oscillation in power system with high penetration of renewable. Elect Power Autom Equip 2023;43(9):152–63.
[35] Wang JZ, Wang S, Zeng B, Lu HY. A novel ensemble probabilistic forecasting system for uncertainty in wind speed. Appl Energy 2022;133:118796.
[36] Wang HZ, Li GQ, Wang GB, Peng JC, Jiang H, Liu YT. Deep learning based ensemble approach for probabilistic wind power forecasting. Appl Energy 2017; 188:56–70.
[37] Quan H, Srinivasan D, Khambadkone AM, Khosravi A. A computational framework for uncertainty integration in stochastic unit commitment with intermittent renewable energy sources. Appl Energy 2015;152:71–82.
[38] Falehi AD. An innovative OANF-IPFC based on MOGWO to enhance participation of DFIG-based wind turbine in interconnected reconstructed power system. Methodologies Appl 2019;23:12911–27.
[39] Ma XY. Scenario analysis and stochastic programming of wing-integrated power systems. Hubei: Wuhan University; 2014.
[40] Freris L, Sasson A. Investigation of the load-flow problem. Proc Inst Electr Eng 1968;115(10):1459–70.
[41] Pai MA. Energy function analysis for power system stability. In: The kluwer international series in engineering and computer science. Boston, MA: Springer; 1989.
[42] Kundu R, Das S, Mukherjee R, Debchoudhury S. An improved particle swarm optimizer with difference mean based perturbation. Neurocomputing 2014;129: 315–33.